Received: 24 January 2020 | Revised: 9 June 2020 | Accepted: 10 June 2020

DOI: 10.1002/ese3.776

RESEARCH ARTICLE

Energy Science & Engineering Open Access

An alternative architecture of the Humphrey cycle and the effect of fuel type on its efficiency

Panagiotis Stathopoulos

Chair of Unsteady Thermodynamics in Gas Turbine Processes, Technische Universität Berlin, Berlin, Germany

Correspondence
Panagiotis Stathopoulos, Chair of Unsteady Thermodynamics in Gas Turbine Processes, Technische Universität Berlin, Müller Breslau Str. 8, 10623 Berlin, Germany.
Email: stathopoulos@tu-berlin.de

Funding information
Deutsche Forschungsgemeinschaft, Grant/Award Number: SFB 1028 - Turbin

Abstract

Conventional gas turbines are a very mature technology, and performance improvements are becoming increasingly difficult and costly to achieve. Pressure-gain combustion (PGC) has emerged as a promising technology in this respect, due to the higher thermal efficiency of the respective ideal gas turbine cycles. The current work analyzes two layouts of the Humphrey cycle for gas turbines with pressure-gain combustion. One layout replicates the classical layout of gas turbine cycles, whereas an alternative one optimizes the use of pressure-gain combustion by ensuring the operation of the combustor at stoichiometric conditions. In parallel, both cycle layouts are studied with two different fuels—hydrogen and dimethyl ether—to account for differences in combustion specific heat addition and its effect on cycle efficiency. The current work concludes with an attempt to benchmark the maximum losses of a plenum to achieve efficiency parity with the Joule cycle, for a given pressure gain over a PGC combustor. It is found that the cycle layout with stoichiometric combustion results in an increase in thermal efficiency of up to 7 percentage points, compared to the classic cycle architecture. Moreover, the thermal efficiency of the new layout is less sensitive to the turbine inlet temperature, especially at low compressor pressure ratios. The study of the two fuels has shown that the larger mass specific heat addition leads to higher cycle thermal efficiency and should be considered during the fuel choice. Finally, the maximum allowable plenum pressure loss that results to efficiency parity with the Joule cycle has been computed for a given combustor pressure gain. For turbine inlet temperatures above 1500°C, pressure gain above 1.6 would allow for at least 20% relative pressure drop in the plenum. The respective pressure gain becomes considerably higher for lower turbine inlet temperatures.

KEYWORDS

gas turbines, Humphrey cycle, hydrogen, pressure-gain combustion

1 | INTRODUCTION

Pressure-gain combustion for gas turbine applications has become a major focus of the research community, mainly due to the potential of the approach for efficiency increase. Experimental studies on resonant pulsed combustors have demonstrated a pressure gain of approximately 3%.[1] At the same time, theoretical and experimental studies of detonative combustion concepts came to the conclusion that pressure gain up to 30% might be possible for pulsed detonation combustion[2,3] and rotating detonation combustion.[4-6]

This great potential has motivated numerous thermodynamic cycle performance studies. Initially, most focused on the generation of thrust from pulse detonation combustors.[2,7-9] They were based on fundamental analyses of the entire gas turbine process, mostly using the ZND (Zeldovich, Neumann, Döring) and Humphrey models. The ZND process models cycle with detonation, while the Humphrey process uses isochoric combustion. Heiser and Pratt took component efficiencies into account to evaluate these processes and concluded that the isentropic expansion efficiency has a major impact on cycle efficiency.[10]

Cambier et al[11] have focused on optimization strategies for pulsed detonation engines (PDEs), while Golmeer et al[12] have presented a hybrid concept of a gas turbine with pulsed detonation combustion (PDC) and conventional combustion. A similar study for a turbojet engine with PDC has been presented by Vutthivithayarak.[13] Stathopoulos[14] analyzed the classic architecture of the Humphrey cycle for gas turbines, while considering a detailed model for blade cooling and an additional compressor for the turbine blade cooling air. To this end, he used a simplified model for the pressure-gain combustion process.[15] The main outcome of this work was that the cycle achieved only limited efficiency advantages at relative low pressure ratios. The main reason for this was the limited specific heat addition in the combustion process and the increased cooling air consumption.

All these studies have neglected the inherent time dependence of the processes. This was addressed by a series of papers by Paxson and Kaemming,[16,17] suggesting ways to integrate the time variation of state variables at the PDC outlet into the thermodynamic process calculations. These suggestions have been adapted and integrated by the author in models of the Humphrey process[18,19] and of the ZND process.[20] In these works, shockless explosion combustion (also see setion 2.2.1) and pulsed detonation combustion have been modeled with a solver for the time-dependent Euler equations with source terms for the reaction process. This model delivered the time variation of all state variables and velocity at the outlet of the combustor. This flow has been subsequently broken down in mass increments that expanded through a turbine. The turbine isentropic efficiency has been computed with a simplified operational map for the total pressure and temperature of each expanding mass increment. These studies have shown that future turbine designs should efficiently convert the high dynamic pressure at the outlet of pressure-gain combustors into work. In any other case, it might be hard to achieve efficiency gains against the conventional Joule cycle.

In the last five years, a number of thermodynamic studies on gas turbines with rotating detonation combustion (RDC) have been published. Nordeen et al[21] and Zhou et al[22] simultaneously developed a model to compute the thermodynamic states along the streamlines in an RDC and adapt the ZND cycle model. Further analytical and simplified models of the RDC combustion process have been developed by Kaemming et al[23] and Mizener and Lu.[24] The latter used their RDC models to estimate the performance of a gas turbine and perform parameter studies. Sousa et al[25] presented a simplified analytical model for the entire gas turbine process with RDC, based on the NASA simulation platform "T-MATS." This work and the experimental work of Naples et al[26-28] and Braun[29] assume a classical process architecture. New process designs have been explored for the first time by Ji et al[30] for gas turbines with RDC.

The current work aims to extend the state of research in three ways. First, past cycle analyses have shown that pressure-gain combustors have the highest performance, when operated with combustible mixtures close to stoichiometry.[10,30,31] This fact and the material limitations posed to the turbine inlet temperature make the study of alternative cycle layouts necessary. The current work proposes such an alternative layout of the Humphrey cycle that takes full advantage of pressure-gain combustion. Second, pressure-gain combustion has been experimentally and numerically studied for a variety of fuels. However, only limited work has been performed so far on the effect of different fuels on the performance of pressure-gain combustion cycles.[32] This is extended here by studying the Humphrey cycle for hydrogen and DME as fuel. Finally, there have been several studies in the past, where a plenum was used between a pressure-gain combustor and a turbine expander. The role of such a plenum is twofold. On the one hand, it is used as an air injection volume to reduce the gas temperature before its entrance in the turbine. This is especially the case, when the upstream pressure-gain combustor operates close to stoichiometry.[27,28,33,34] On the other hand, conventional turbines experience a considerable drop of their isentropic efficiency, when they operate at the outlet of pressure-gain combustors. The strong variations of pressure, temperature, and velocity cause excessive aerodynamic losses and could negate all thermodynamic gains harvested from pressure-gain combustion.[35,36] A plenum can be used to condition the incoming flow in a turbine and minimize the aerodynamic losses in it. The current work systematically studies the trade-off between combustor pressure gain and the maximum allowable thermodynamic losses in this plenum. It thus provides a first benchmark for the maximum

allowable losses in the plenum, to achieve an efficiency increase with a combination of pressure-gain combustion and conventional turbines.

2 | MODELS AND METHODS

2.1 | Overall cycle models

Figure 1 shows the two alternative layouts of the Humphrey cycle studied in the current work. Layout 1 is the same as in.[14] Here, the whole compressor air flow is directed in the combustor. A small additional air compressor delivers cooling air to the first turbine stator row. In this layout, the equivalence ratio is directly linked to the turbine inlet temperature. Material limitations therefore set an upper operational limit for the combustion equivalence ratio and thus on the possible pressure gain of the combustor.

This limitation is overcome with layout 2 (see Figure 1B). Here, the combustor is fed with air from an air bleed in the compressor. The remaining air is directed through additional compressor stages to a plenum downstream of the combustor. It mixes with the exhaust gas of the combustor to reduce its temperature to the defined turbine inlet temperature. Part of this air mass flow is also used to cool the first turbine stator row. The pressure ratio of these additional compressor stages (C_2 in Figure 1B) is defined through the pressure gain of the combustor. In this layout, the fuel flow rate is chosen so that the energy balance over the combustor and the plenum results to the defined turbine inlet temperature (T_6 in Figure 1B). The air mass flow rate directed to the combustor ($\dot{m}_2$ in Figure 1B) is chosen according the set respective equivalence ratio, thus offering the freedom to choose the value of the latter independently.

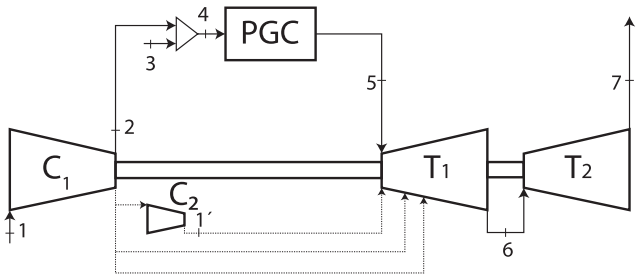

(A) Layout 1

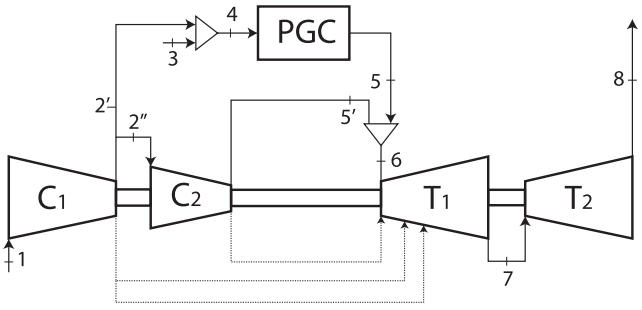

(B) Layout 2

FIGURE 1 Humphrey cycle layouts

Aspen plus has been used in the current work to model the cycles, due to its extensive material properties database. The material properties of the working fluid were computed with the RK-BS model, and its composition changed from the compressor to the turbine. Both the expansion process in the rotor rows and compression were assumed to be adiabatic processes with a constant isentropic efficiency. Both layouts of the Humphrey cycle have been compared to the Joule cycle with turbine cooling, presented in Figure 2. Table 1 shows the model parameters in detail.

2.2 | Thermodynamic representation of pressure-gain combustion

The heat addition process in the combustor has been represented in ASPEN Plus by a user defined function, based on an adaptation of the model presented by Nalim.[15] The pressure-specific volume diagram of the subprocesses taking place in the combustor according to the implemented model is presented in Figure 3, along with the rest of the ideal Humphrey cycle (corresponding to layout 1). The model divides the heat addition process in two parts. In the first part, an ideal constant volume heat addition raises the pressure and temperature from the inlet conditions (A) to the intermediate thermodynamic state (B).

From the assumption of a perfect gas with constant material properties (computed iteratively at average temperature and pressure of the working medium) in the combustion chamber, the temperature change ($T_B - T_A$) can be computed by Equation (1). Here, Q is the total heat addition from the fuel and $\dot{m}$ is the mass flow rate entering the combustor.

$$Q = \dot{m} \cdot c_v \cdot \left(T_B - T_A\right) \tag{1}$$

By also assuming that the working medium is a perfect gas, the respective pressure change ($p_B - p_A$) can be calculated by Equation (2).

$$\frac{T_B}{p_B} = \tag{2}$$

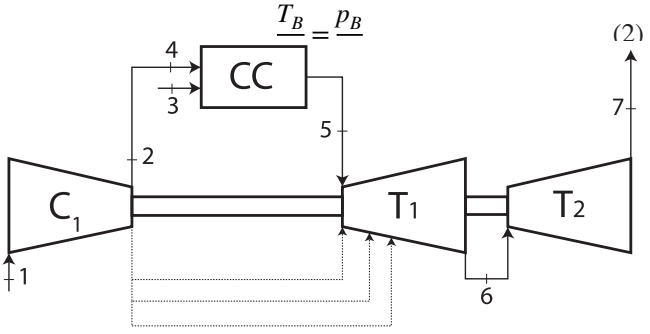

FIGURE 2 Schematic of the Joule reference cycle

TABLE 1 Model parameters and assumptions

	Symbol	Layout-1	Layout-2	Joule
Compressor	η_{isC}	0.9	0.9	0.9
	Π_{C1}	10-40		
Combustor	η_{isPGC}	0.6-1		N/A
Plenum	δp_{plenum}	N/A	0%-40% of p_5	N/A
Turbine	η_{isT}	0.9	0.9	0.9
	$\Pi_{T-stage}$	$p_5^{-\frac{1}{3}}$		
	TIT	1300-1500-1700		
	δp_{mix}	1%		

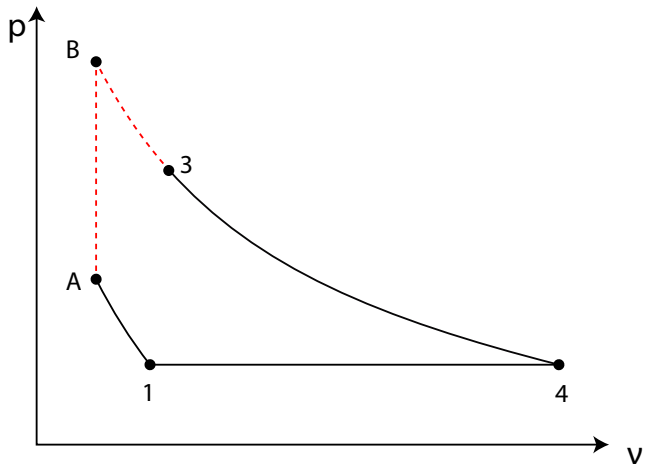

FIGURE 3 Pressure-specific volume diagram of the combustor model (dashed line) incorporated in the ideal Humphrey p-v diagram

Generally, pressure-gain combustion and specifically constant volume combustion are realized through time-dependent combustors. The model aims at representing this by an equivalent thermodynamic state at the exit of the combustion that could be then used for a steady-state model of an open thermodynamic system. In order to do that, the flow work consumed to expel the products of the constant pressure heat addition process (A-B) must be accounted for. This is done by an expansion process from the end state of the heat addition process (B) to the equivalent exit state of the combustor (3). By using the basic assumption that the process A-3 represents a heat addition process in an open thermodynamic system, one can compute the temperature at point 3 through Equation (3).

$$Q = \dot{m} \cdot c_p \cdot \left(T_3 - T_A\right) \tag{3}$$

Finally, the pressure at point 3 can be computed through the basic equations that describe an expansion process with a given isentropic efficiency ($\eta_{is_{PGC}}$). This isentropic efficiency will be used in this work to account for all relevant irreversibilities in the combustor-internal expansion process. Equation (4) gives the respective result.

$$\frac{p_3}{p_B} = \left(1 - \frac{1 - \frac{T_3}{T_B}}{\eta_{is_{PGC}}}\right)^{\frac{\gamma}{\gamma-1}} \tag{4}$$

Based on Equations (1)-(4), one can also define the combustor pressure ratio as the ratio $\frac{p_3}{p_A}$.

2.2.1 | Model calibration and validation

The presented heat addition model is a simple representation of the very complex phenomena taking place in various quasi-constant volume combustors, like pulsed resonant or shockless explosion combustors. The model uses the average material properties for the heat addition (A-B in Figure 3) and internal expansion processes (B-3 in Figure 3). This averaging is performed by computing the material properties (c_v, c_p, and γ) of the reactants at the combustor inlet temperature (T_4 in Figure 1) and these of the products at an intermediate temperature (T_{int}). The average value of c_v, c_p, and γ is subsequently used in Equations (1)-(4). The aforementioned intermediate temperature (T_{int}) and the isentropic efficiency ($\eta_{is_{PGC}}$ in Equation 4) of the internal expansion in the combustor are the two parameters that must be calibrated.

The reference data for this calibration can be acquired through experiments at the same inlet combustor conditions, or through simulations with a validated model. The time-resolved data of the pressure, temperature, and velocity at the combustor outlet can be used to compute the mass-averaged total temperature and pressure with Equations (5) and (6).

$$T_{tout} = \frac{\int_{t_0}^{t_{end}} \dot{m}(t) \cdot T_t(t) dt}{\int_{t_0}^{t_{end}} \dot{m}(t) dt} \tag{5}$$

$$p_{tout} = \frac{\int_{t_0}^{t_{end}} \dot{m}(t) \cdot p_t(t) dt}{\int_{t_0}^{t_{end}} \dot{m}(t) dt} \tag{6}$$

The resulting T_{tout} and p_{tout} are inserted in Equations (1)-(4). The values of T_{int} and $\eta_{is_{PGC}}$ are computed from these equations iteratively so that the model delivers $p_3 = p_{tout}$ and $T_3 = T_{tout}$ for the same combustion equivalence ratio.

This validation process has been carried out in the current work with previously published data from detailed simulations of shockless explosion combustion.[18] Shockless explosion combustion (SEC) is a pressure-gain combustion concept that uses simultaneous autoignition. Chemical and acoustic time scales in the combustor are exploited to realize the four phases of this cyclic process. Phase 1 starts

with the homogeneous autoignition and the generation of the respective pressure wave. It ends when this pressure wave reaches the combustor open end. Phase 2 starts when this wave is reflected as a suction wave and ends at its arrival at the closed combustor end. Phase 3 commences after its reflection at the closed combustor end that enables refilling of the tube and finishes when the suction wave reaches the open combustor end. During phase 4, the suction wave gets reflected again as a weak pressure wave at the open end and reaches the closed end of the combustor when homogeneous ignition takes place. More details on the SEC process can be found in.[18,37,38]

The simulations for the SEC process, used for the aforementioned calibration, were carried out with the model of the time-resolved 1D-Euler equations with source terms for the detailed chemistry, presented in.[18] Details about the numerical treatment of the gas dynamics and chemistry problem can be found in the work of Berndt.[39] The length of the tube was discretized in 100 cells, and the time resolution was $\Delta t = 10^{-6}$ s. For every time step, the complete state (temperature, pressure, velocity, composition, etc) was calculated with a detailed reaction kinetic model[40] for the case with hydrogen as fuel.

Figure 4A,B presents the mass-averaged total temperature and the combustor pressure gain based on the mass-averaged total pressure, all computed from results of the simulations in.[18] Figure 4C shows the results of the calibration for the ϕ value, where T_{int} was iteratively varied until the ϕ calculated from the simplified model matched the one from the detailed simulation. Simultaneously with this variation, the η_{isPGC} was computed and is presented in Figure 4D. It can be seen that the model can represent the general trends in the combustor, while the value of T_{int} varied only slightly between 2550 and 2650°C for all calibrated cases. Figure 4D shows that the expansion process in the combustor generates some entropy and the equivalent isentropic efficiency of this expansion process (η_{isPGC}) lies between 0.87 and 0.91, for the studied cases. No correlation between η_{isPGC} and the combustor inlet pressure can be observed. Although these values come from a detailed model that neglects friction and heat transfer to the combustor walls, they compare well with the values expected from literature.[3]

In the current work, T_{int} has been kept equal to 2600°C, as this value delivers very representative results for the material properties in all relevant operational conditions. However, the value of η_{isPGC} is considered a free parameter, since it has a much larger

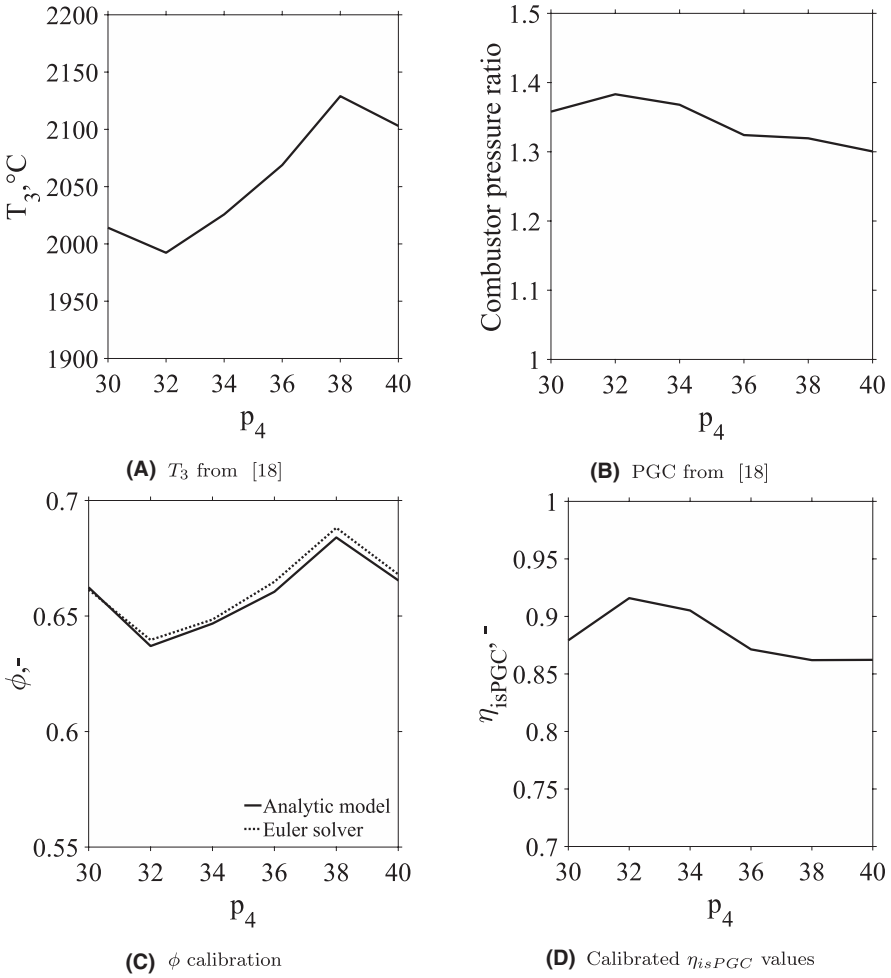

FIGURE 4 Upper two figures: Mass-averaged total temperature and pressure gain as a function of the inlet pressure for the SEC simulations presented in.[18] Lower two figures: Equivalence ratio matching results during the calibration of T_{int} and η_{isPGC} values for the simplified model

effect on the actual pressure gain achieved from the combustor. As a result, it can be used to represent different configurations of quasi-constant volume combustors and provide a benchmark for their design, based on the computed cycle performance.

2.3 | Secondary air model

The secondary air model is based on[41-44], and it has been integrated in the ASPEN Plus cycle model with design specifications modules. For a given temperature and mass flow rate of the hot gas entering the stage in question, it computes the convective and film cooling air mass flow rate and the associated pressure losses for given cooling air and blade temperatures.

The expansion process in each turbine stage is split into three steps. The first computes the temperature and the pressure of the hot gas at the stator exit. This is the result of a mixing process between the hot gas at the stator inlet and the stator cooling air. A pressure loss coefficient (δp_{stage} in Table 1) is used to calculate the exit pressure. The second part comprises the working medium expansion in the rotor. The exit conditions of this expansion process are computed with the help of a fixed isentropic efficiency. In the third step, the rotor cooling air stream is mixed with the expanded gas to form the gas that exits the stage. The cooling air flow is computed by assuming a constant external Stanton number St_g. The parameters of the turbine cooling model used in the current work can be seen in Table 2. The blade temperature is set equal to 1100 K for all computations. The turbine expansion ratio ($\Pi_{T-stage}$) is equally distributed among the three stages. As a result, only the first three blade rows have to be cooled. Depending on the cycle layout and the pressure gain across the combustor, cooling air may be provided to the turbine stages from different points across the compressor, as shown in Figure 1. In layout 1, a small cooling air compressor delivers air at the first turbine stator row. In layout 2, an air bleed supplies rows 2 and 3 with cooling air, while the air for the first stator row is taken from the compressor outlet.

2.4 | Simulation procedure

The current work aims to study the effect of cycle layout and fuel on the cycle performance and compare the latter to that of the Joule cycle. In layout 1 of the Humphrey cycle, the mass flow rate of fuel is controlled by the turbine inlet temperature and the mass and energy balance across the combustor. As a result, the combustor equivalence ratio and pressure gain are defined directly from its boundary conditions. In layout 2, the combustor equivalence ratio is directly defined. Here, the turbine inlet temperature is the temperature at point 6 in Figure 1B, at the exit of the plenum that mixes the one air stream (5′ in Figure 1B) and the exhaust stream of the combustor (5 in Figure 1B). The mass flow of the two air streams (2′ and 2″ in Figure 1B) is iteratively calculated along with the fuel mass flow rate to match both the defined turbine inlet temperature and the chosen combustor equivalence ratio. In layout 2, the outlet pressure of the compressor second stage (C_2 in Figure 1B) is set equal to the combustor outlet pressure.

TABLE 2 Cooling system model parameters based on the model from[41]

Parameter	Symbol	Value
Cooling efficiency	$\eta_{Cooling}$	0.9
Film cooling effectiveness	ε_F	0.4
Level of technology constant	C	0.045
Pressure loss constant	K	0.07
Blade temperature	T_{bl}	1100 K

The simulations are carried out for three turbine inlet temperatures and varying pressure ratio of the compressor's first stage (C_1 in Figures 1 and 2) as shown in Table 1. Each cycle layout has been analyzed for hydrogen and DME as a fuel. Hydrogen is the major fuel used for pressure-gain combustion applications[4] and is thus considered a reference fuel for the present study. Dimethyl ether (DME) was chosen as a fuel due to its excellent ignitability[37,38] and is prior use for shockless explosion combustion studies. It is a promising alternative fuel that can be produced as e-fuel based on renewable power (PtG)[45] or from biomass.[46] The impact of the plenum pressure drop and the combustor performance in the two Humphrey cycle layouts is presented with the help of sensitivity analyses at chosen design points of the cycles. In these cases, all cycle parameters are kept constant, while the studied parameter (plenum pressure drop or combustor isentropic efficiency) is varied in the range of values presented in Table 1.

3 | RESULTS

Figure 5 presents the cycle thermal efficiency for all studied cycles and for the two fuels in question. The first observation for both fuels is that the Humphrey layout 2 has the highest thermal efficiency in the range of parameters studied here. The change from layout 1 to layout 2 results in a thermal efficiency increase of up to 7 percentage points (See Figure 5A at Π_C of 25). Moreover, the thermal efficiency of layout 2 is less sensitive to the turbine inlet temperature especially at low Π_C values, thus making cycles with relatively low TIT values very attractive. Finally, the two graphs on Figure 5 make clear that the fuel type plays also an important role. In fact, the Humphrey cycles with DME have slightly lower efficiencies, compared to the ones with hydrogen. The following paragraphs will provide an explanation of these observations.

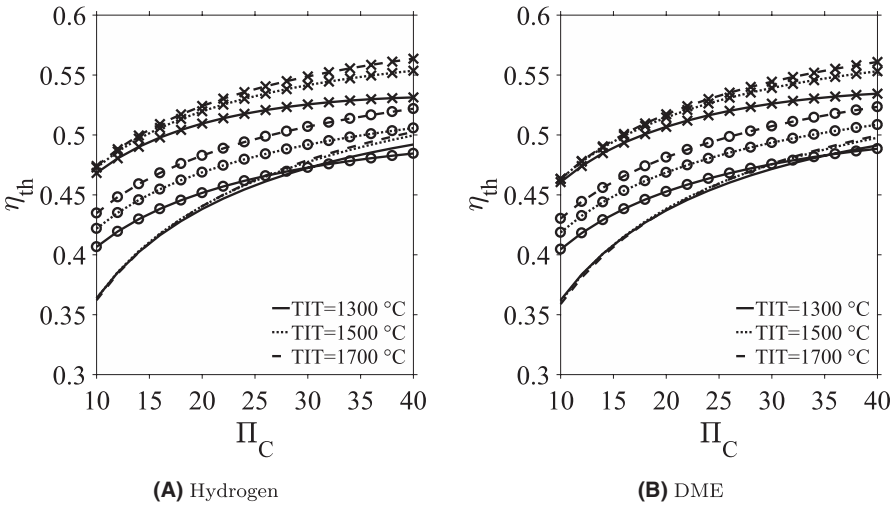

(A) Hydrogen **(B)** DME

FIGURE 5 Efficiency of the Humphrey cycle layouts and the Joule cycle for two different fuels. Lines with ○—layout 1, lines with ×—layout 2, and lines without symbol—Joule cycle

The considerable increase in efficiency for layout 2 can be directly connected to the combustor pressure gain, as presented in Figure 6. For both fuels, layout 2 enables the combustor to operate at stoichiometric conditions thus maximizing its pressure gain. The turbine inlet temperature is controlled from the amount of air by-passed to the plenum. As a result, combustor pressure gain is the same irrespective of the chosen turbine inlet temperature. It drops with increasing Π_C, because the combustor inlet temperature also increases with Π_C. In contrast, pressure gain in layout 1 increases with the turbine inlet temperature, because the combustor moves to richer mixtures (see also[14]). The same can be said for the comparison of the Humphrey cycle efficiency for the two studied fuels. Hydrogen results in a slightly higher pressure gain then DME and thus also a slightly higher cycle thermal efficiency. This effect is a result of the larger mass specific heat addition of hydrogen (3.5708 $MJ/kg_{mixture}$), when compared to that of DME (2.4476 $MJ/kg_{mixture}$) at stoichiometric combustion.

Nevertheless, the above observations cannot explain why the cycle efficiency in layout 2 is almost the same for all TIT values at low Π_C and the difference increases for higher Π_C values. To understand this, one has to examine the air distribution within the cycle, presented in Figure 7 for the cycle that uses hydrogen. From Figure 7B, one can observe that the cooling air percentage for 1300°C is more than doubled between the cycles with Π_C 10 and 40. Although the rate of increase is similar for the cycles with higher TIT values, the relative increase is not so high thus having a smaller impact on the overall efficiency of the cycle. By the same token, the air part that goes through the combustion chamber and experiences the respective combustor induced pressure increase is only between 21% and 32% for a TIT of 1300°C. As a result, between 65% and 75% of the air has to go through the second compressor stage to land in the plenum and cool the exhaust gas of the combustion chamber. The compression of this part consumes work, thus having an impact on the overall efficiency of the cycle. In contrast to this, the cycles with higher TIT values direct a larger percentage of air through the combustion chamber, thus achieving a higher efficiency, especially for relatively large pressure ratios. The Humphrey cycle layout 2 results

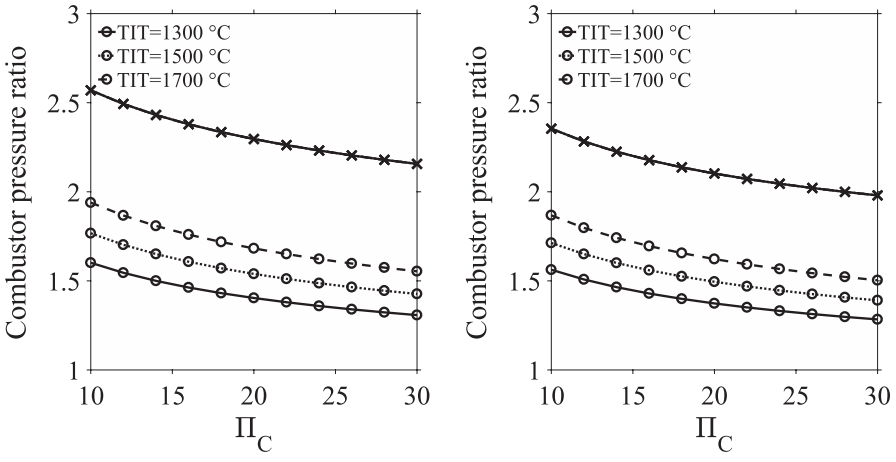

(A) Hydrogen **(B)** DME

FIGURE 6 Pressure gain of the Humphrey cycle layouts for two different fuels. Lines with ○—layout 1, and lines with ×—layout 2

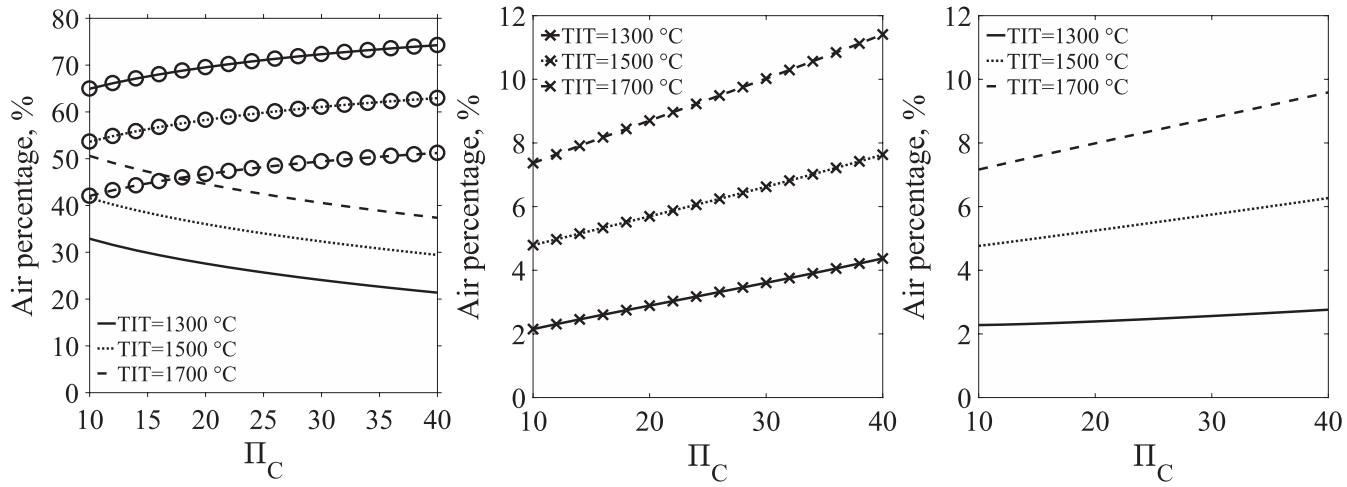

FIGURE 7 Air distribution between combustion chamber, plenum, and turbine cooling air for layout 2 and the Joule cycle with hydrogen. All values are percentage values of the air entering the compressor. Lines with ○—plenum air, and lines with ×—cooling air

in a higher cycle efficiency not only through the more efficient heat input process, but also through the lower turbine outlet temperature and exhaust gas losses, as can be seen in Figure 8. Layout 2 of the Humphrey cycle has consistently the lowest exhaust temperature for all studied pressure ratios. Similarly, layout 1 has lower values than the Joule cycle.

The last relevant cycle parameter for the intended comparison is the specific work generation of the cycles in question, which is presented in Figure 9 for the two fuels in question. For both fuels, layout 1 of the Humphrey cycle demonstrates the highest specific work generation. Interestingly, when comparing the specific work generation of layout 2 with that of the Joule cycle, it becomes clear that the latter results in some cases in a higher value for high Π_C values. This is the case for TIT values between 1300°C and 1500°C.

3.1 | Sensitivity analyses

Pressure-gain combustion concepts that can be modeled with the presented model (like shockless explosion combustion[18] or pulsed resonant combustion[2]) result in considerable entropy generation in their internal expansion process. The influence of this entropy generation on the performance of layout 2 cycles will be studied by varying the isentropic efficiency of the combustor-internal expansion process between 0.6 and 1 (as shown in Table 1). Another assumption in the previously presented models is that the plenum in Humphrey cycle layout 2 causes no pressure loss. In reality, this component mixes a steady stream of air (stream at point 5′ in Figure 1B) with the flow that leaves the pressure-gain combustor (stream at point 5 in Figure 1B). In real PGC operation, the parameters of the latter flow stream (pressure, temperature, velocity) will vary with time. As a result, the respective mixing process in the

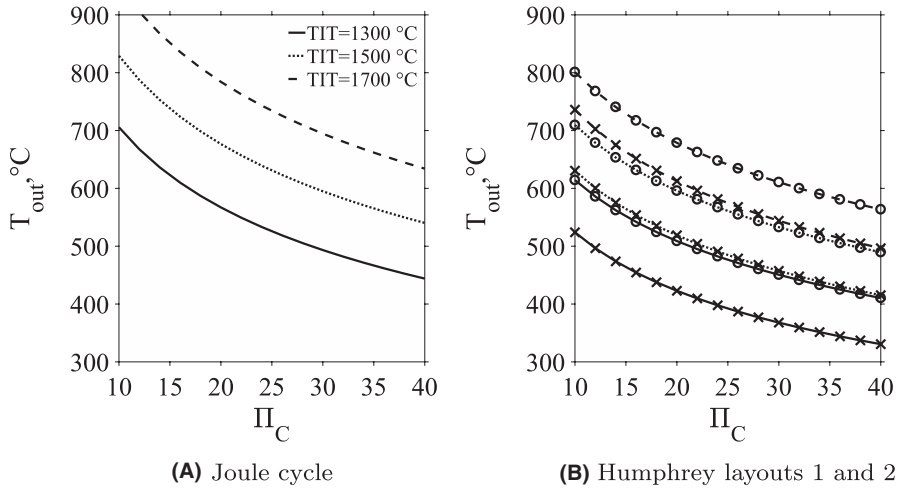

FIGURE 8 Turbine exhaust temperature for the Joule cycle and the two Humphrey cycle layouts and the case with hydrogen. Lines with ○—layout 1, lines with ×—layout 2, and lines without symbol—Joule cycle

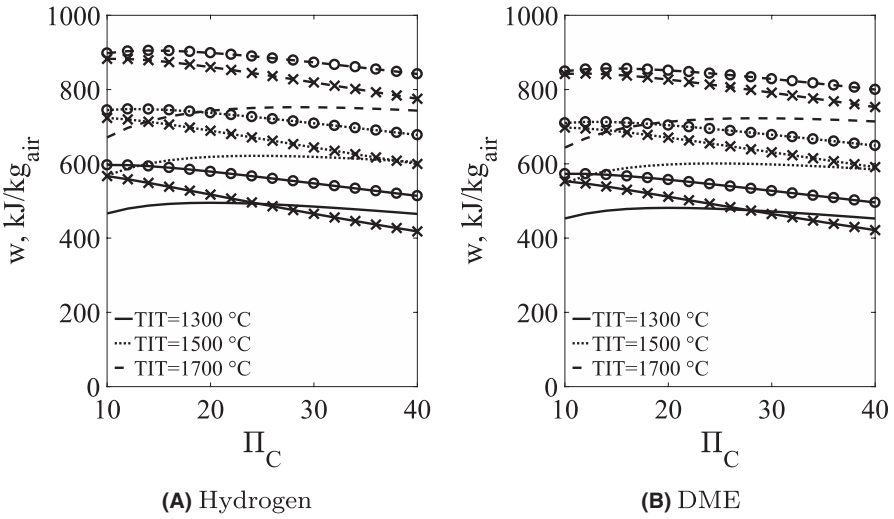

FIGURE 9 Specific work generation of the Humphrey cycle layouts and the Joule cycle for two different fuels. Lines with ○—layout 1, lines with ×—layout 2, and lines without symbol—Joule cycle

plenum will cause a pressure drop that could have a significant impact on cycle performance. This pressure drop is the second parameter studied in the current section.

Figure 10 presents the effect of varying plenum pressure drop on the efficiency of the Humphrey cycle layout 2. This is done once for a given value of the TIT (1500°C) and four values of the Π_C (Figure 10A) and once for a given Π_C and three TIT values (Figure 10B). The reference pressure drop in all diagrams is 20% of the plenum inlet pressure. As a result, −100% refers to $\delta p_{plenum} = 0$ and +100% to $\delta p_{plenum} = 40\%$. Both diagrams show that the thermal efficiency of cycles with low Π_C and TIT values is more sensitive to changes in actual plenum pressure drop, although this difference is rather small. Apart from this, one can see that doubling the pressure drop over the plenum in layout 2 results generally in a decrease in the efficiency of the cycle of approximately 4%.

An increase in the plenum pressure drop reduces the turbine inlet pressure and impacts cycle efficiency in multiple ways. On the one hand, the lower turbine inlet pressure reduces the cooling air pressure—and thus its temperature—for the first turbine stator row. The lower cooling air temperature results also in a decrease in its mass flow for the same blade material temperature, as can be seen in Figure 11. From the same figure, it can be seen that the lower cooling air pressure also reduces the necessary compressor work. However, the impact on compressor work is by far weaker than the reduction in turbine work caused from the resulting lower expansion ratio. Given that the fuel flow rate does not change with the plenum pressure drop, this also explains the observed drop in cycle efficiency of layout 2 with increasing plenum pressure drop.

Figure 12 presents the effect of changes in η_{isPGC} on the efficiency of the Humphrey cycle layout 2. This is done again, for a given value of the TIT (1500°C) and four values of the Π_C (Figure 10A) and for a given Π_C and three TIT values (Figure 10B). The reference η_{isPGC} value in all diagrams is 0.8. Unlike the case with the plenum pressure drop, the cycle efficiency is more sensitive on the value of η_{isPGC} for cycles with low Π_C. In fact, a change from a value of 1 to 0.6 reduces the cycle efficiency by 17% in a cycle with $\Pi_C = 10$, while this efficiency reduction is 8% if the cycle has a $\Pi_C = 40$. For a given Π_C value, the TIT has a rather limited impact on the sensitivity of the cycle efficiency on η_{isPGC}.

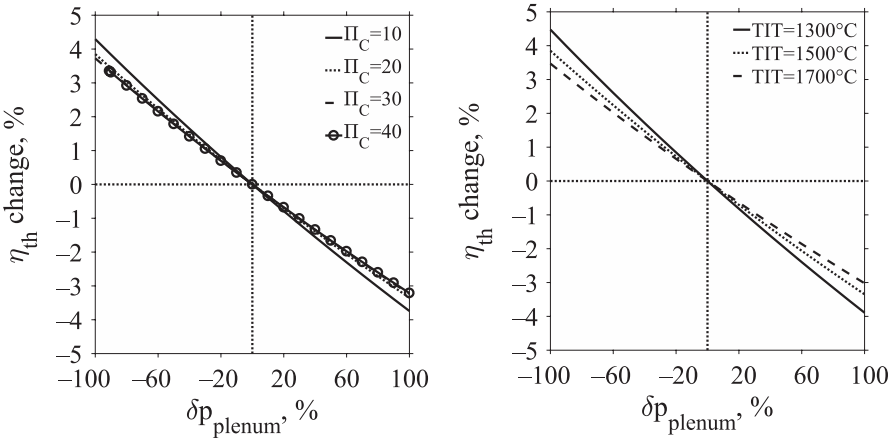

FIGURE 10 Sensitivity of layout 2 thermal efficiency on the plenum pressure drop

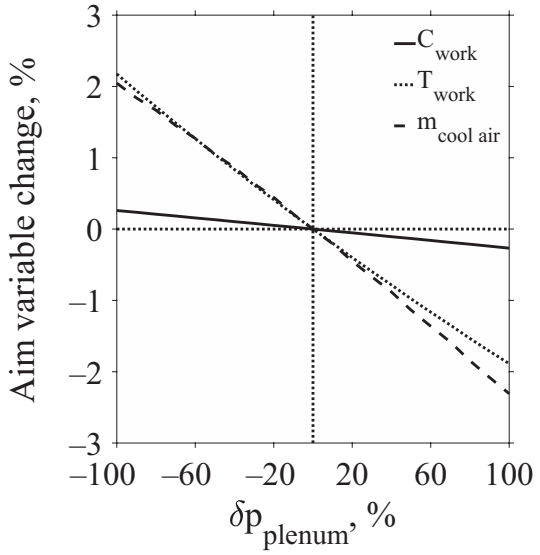

FIGURE 11 Sensitivity of compressor work, turbine work, and cooling air percentage for $\Pi_C = 20$ and TIT = 1500°C, of Humphrey cycle layout 2

Changes of the η_{isPGC} have a direct impact on the pressure gain of the combustion chamber. Based on the model equations for the PGC combustor (1)-(4), the combustor outlet temperature is defined by the respective energy balance for an open thermodynamic system (see Equation 3). Its outlet pressure is, however, directly connected to the isentropic efficiency of the internal expansion process. As a result, the maximum possible pressure gain will occur, when this expansion process is isentropic. This is presented in Figure 13 for four Π_C values at a TIT of 1500°C. Figure 13A reveals that changing η_{isPGC} from 1 to 0.6 will effectively eliminate any pressure gain for the combustor in the cycle with $\Pi_C = 40$. The combustor of the cycle with $\Pi_C = 10$ reaches this point of no pressure gain at a slightly lower η_{isPGC}, due to its lower inlet temperature. However, the relative changes in combustor pressure gain are practically the same irrespective of the cycle pressure ratio, as can be seen in Figure 13B. Here, the reference value of η_{isPGC} is 0.8 and we can see that a change of 25% in its value cases a similar change in the combustor pressure gain.

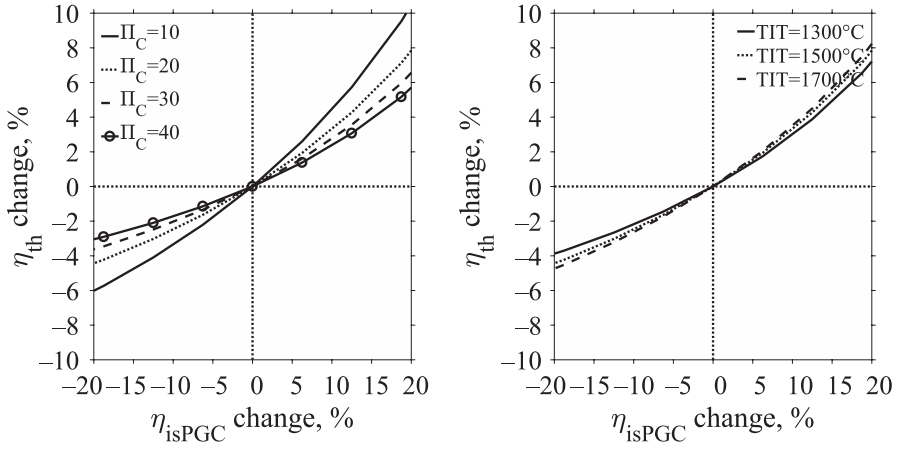

(A) Various Π_C, TIT=1500 °C

(B) Various TIT, $\Pi_C = 20$

FIGURE 12 Sensitivity of layout 2 thermal efficiency on the isentropic efficiency (η_{isPGC}) of the PGC-combustor-internal expansion process

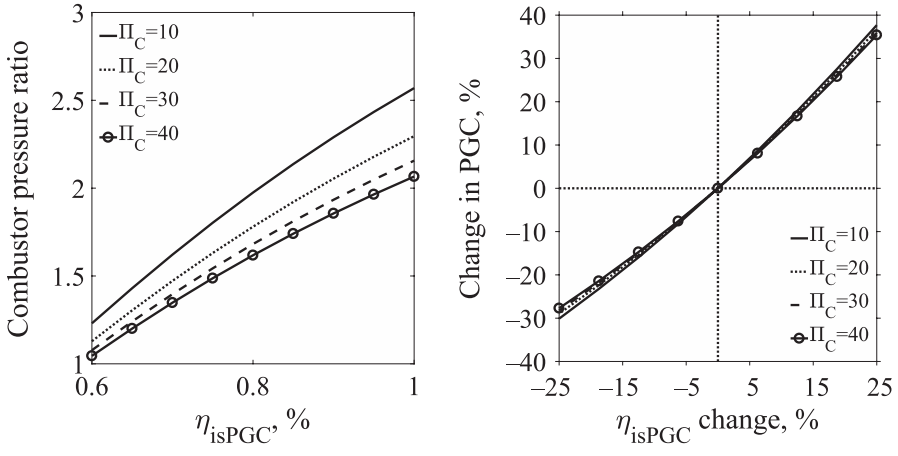

(A) Combustor pressure ratio

(B) Combustor pressure ratio sensitivity

FIGURE 13 Combustor pressure ratio values and sensitivity as a function of η_{isPGC} for the Humphrey cycle layout 2 with $\Pi_C = 20$ and TIT = 1500°C

The lower pressure gain due to the lower η_{isPGC} has some additional effects on the cycle, when compared to the plenum pressure drop. The combustor pressure gain defines the pressure at points 5 and 5′ of the cycle (see Figure 1B), which in turn define the pressure ratio of the second compressor stage (C_2). Lower pressure gain will directly reduce the pressure ratio of this compressor stage and hence lower the temperature of the plenum air at point 5′ and for the turbine cooling air. At the same time, the combustor inlet conditions, its outlet temperature, and the TIT (T_6 in Figure 1B) do not change (see Equations 1-4). The first result of these changes is a reduction of the cooling air percentage, due to the lower cooling air temperature. Similarly, the amount of air that will be directed to the plenum will be reduced, since it has a lower temperature, and all other temperatures around the plenum stay the same. This will in turn increase the amount of air directed to the combustion chamber. Since the equivalence ratio is held constant to $\phi = 1$, also the fuel flow will increase as a result. Finally, a lower η_{isPGC} will simultaneously reduce the compressor work consumption and the turbine work generation. Specifically, the change in their difference and its connection to the total fuel flow are interesting for the cycle efficiency. The former ($T_{work} - C_{work}$) will decrease for decreasing η_{isPGC}, while the latter (m_{fuel}) will increase, thus resulting in a drop of the cycle efficiency. The intensity of the described changes in all these cycle parameters is presented in Figure 14 for the case of cycle layout 2 with $\Pi_C = 20$ and TIT = 1500°C.

3.2 | Benchmarking the PGC combustor and the plenum losses

From the last section, it becomes clear that the plenum pressure loss and the isentropic efficiency of the combustor-internal expansion process have a significant impact on cycle efficiency. In reality, η_{isPGC} can be influenced only partially through influencing the operational conditions (temperature, equivalence ratio, and pressure) and the design of the combustor. However, once a PGC combustor is integrated in a cycle, its operational conditions are fixed. As a result, only the detailed design of the combustor and the gas dynamic phenomena during the internal expansion process can change the η_{isPGC} value. In a similar manner, only the design and the actual operational conditions of the plenum will define the pressure drop during its operation. It is thus interesting to compute the values of these parameters, for which the Humphrey cycle layout 2 has the same efficiency with the Joule cycle, when the TIT and Π_C values are the same for both.

Figures 15 and 16 show these combinations for several Π_C values in the cycle operating with hydrogen and having TIT values of 1300°C, 1500°C, and 1700°C, respectively. Since most literature refers to the expected pressure gain of a pressure-gain combustor, these figures also present the combination of combustor pressure ratio and plenum pressure drop for efficiency parity of the aforementioned cycles. With these figures, one can compute the maximum pressure drop that the plenum is allowed to generate for a given combustor pressure ratio to achieve efficiency parity. If lower pressure drops are possible at this combustor pressure ratio, an efficiency advantage is possible for the Humphrey cycle layout 2. The same goes for higher pressure ratios at the same plenum pressure drop. In other words, in all these diagrams, the surface to the right of the presented curves represents combinations of the values that result in higher efficiency of the Humphrey cycle layout 2.

Focusing on the results for a TIT of 1300°C (Figure 15), the first observation is that for the same η_{isPGC} or combustor pressure ratio, higher compressor pressure ratios reduce the maximum allowable plenum pressure drop for efficiency parity. More specifically, the Humphrey cycle achieves the same efficiency with the Joule cycle at a combustor pressure ratio of 1.15 for all cases, if the plenum pressure drop is neglected. A combustor pressure ratio of 1.4 already allows for a pressure drop of 8% for the cycle with $\Pi_C = 40$ and 16% for the cycle with $\Pi_C = 10$. Moreover, the cycle with $\Pi_C = 40$ cannot reach efficiency parity for plenum pressure drops beyond

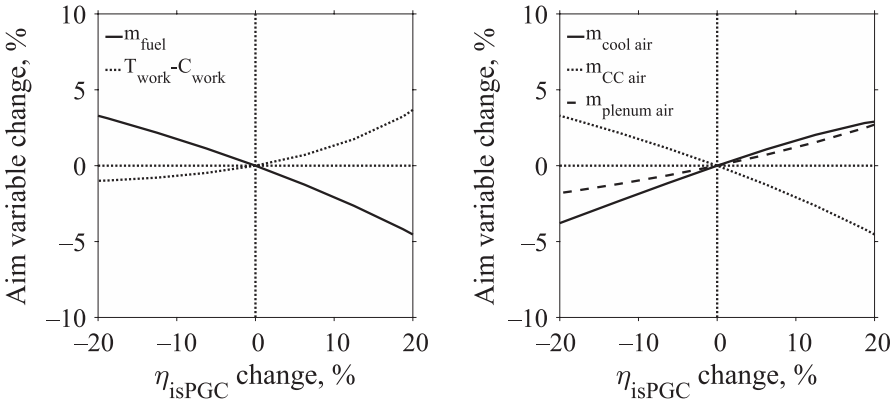

(A) Work differential and fuel flow **(B)** Air flows

FIGURE 14 Sensitivity of the air work difference between turbine and compressor, the fuel flow rate and the air flows on the η_{isPGC} value for the Humphrey cycle layout 2 with $\Pi_C = 20$ and TIT = 1500°C

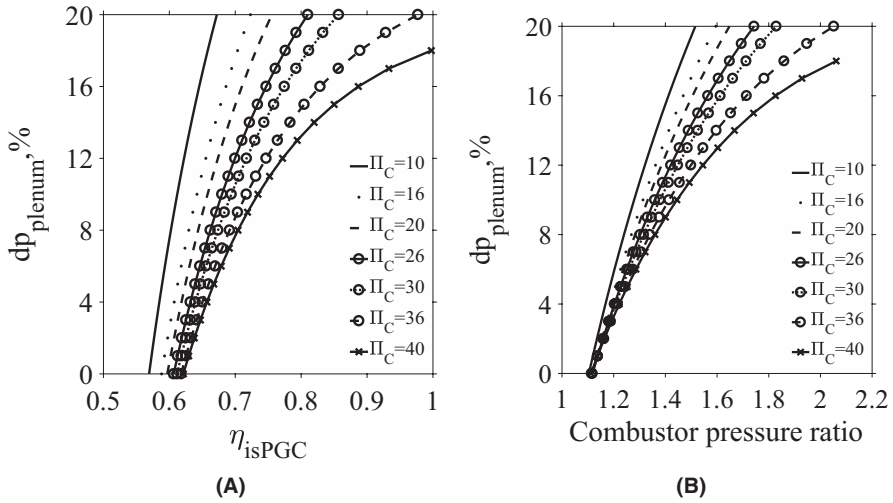

FIGURE 15 Values of η_{isPGC}, plenum pressure drop, and combustor pressure ratio, for which the Humphrey cycle layout 2 has the same thermal efficiency as an equivalent Joule cycle with the same Π_C. All cycles in the diagrams have TIT = 1300°C and use hydrogen as a fuel

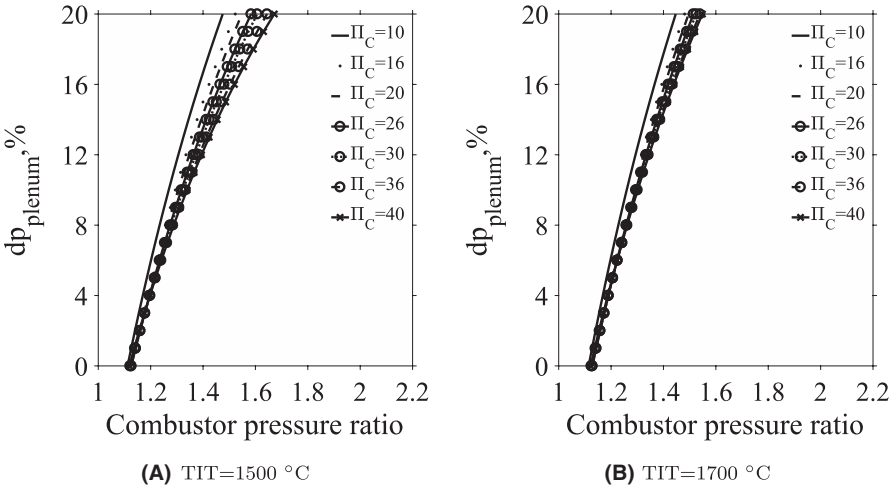

FIGURE 16 Values of plenum pressure drop and combustor pressure ratio, for which the Humphrey cycle layout 2 has the same thermal efficiency as an equivalent Joule cycle with the same Π_C. The cycles in the left have a TIT = 1500°C and those on the right a TIT = 1500°C. In all cases, hydrogen was the considered fuel

18%, while the cycle with $\Pi_C = 36$ reaches marginally efficiency parity at a plenum pressure drop of 20% and an ideal combustor ($\eta_{isPGC} = 1$). The observed behavior for the low TIT cycles was expected (see also Figure 5), mostly because of the strong influence of the turbine expansion ratio and the importance of its efficiency in these cycles.

This picture changes for higher TIT values, as can be seen in Figure 16. Here, the importance of the compressor pressure ratio becomes less the higher the TIT value. Moreover, the higher the TIT value, the higher the allowed plenum pressure drop for a given combustor pressure ratio. This trend seems to saturate for a TIT of 1700°C, and much smaller changes are expected for even higher TIT values. Specifically, for TIT = 1500°C, a combustor with a pressure ratio of 1.6 will result in efficiency parity at a plenum pressure drop of 20%, even for a cycle with $\Pi_C = 40$. The pressure ratio drops to 1.5 for the cycle with TIT = 1700°C. The expected mass-averaged TIT values for state-of-the-art turbine expanders lie between 1500°C and 1700°C. At the same time, pressure-gain combustors are expected to achieve pressure ratios between 1.2 and 1.6.[2] Based on the results presented in Figure 16, the design of devices that connect these pressure-gain combustors with the downstream turbines should result in pressure drops below 20%, in order for the respective Humphrey cycle to achieve efficiency gains against an equivalent Joule cycle.

4 | CONCLUSIONS

The current work has extended the results of the work presented in,[14] by introducing an new cycle architecture that exploits all advantages of pressure-gain combustion for gas turbines. It was found that the new layout (2) brings about an increase in thermal efficiency of up to 7 percentage points, compared to the classic Humphrey cycle layout (1). The reason behind this observation is the considerably higher combustor pressure gain, achieved in the new cycle layout. Another significant observation is that the thermal efficiency of the new layout is less sensitive to the turbine inlet temperature, especially at low Π_C values. This result is very important for the economics behind the respective gas turbines, since not too sophisticated cooling technologies will be necessary

for their implementation. At the same time, the classic cycle (layout 1) demonstrated the highest specific work generation. The specific work generation of layout 2 was comparable to that of the equivalent Joule cycle. Based on this result, it can be stated that the proposed layout is better suited for stationary applications.

In what concerns the effect of fuel on the performance of the Humphrey cycle layouts, it has been shown that the larger mass specific heat addition of hydrogen (3.5708 MJ/$kg_{mixture}$, DME 2.4476 MJ/$kg_{mixture}$) results in a higher pressure gain and also higher cycle thermal efficiency.

The sensitivity analyses have shown that the layout 2 Humphrey cycle efficiency is more sensitive on the value of η_{isPGC} for cycles with low Π_C. In fact a change from a value of 1 to 0.6 reduces the cycle efficiency by 17% in a cycle with $\Pi_C = 10$, while this efficiency reduction is 8% if the cycle has a $\Pi_C = 40$. For a given Π_C value, the TIT had a rather limited impact on the sensitivity of the cycle efficiency on η_{isPGC}. These results motivated a study to compute the maximum allowable plenum pressure loss for a given combustor pressure gain, in order to achieve efficiency parity between the layout 2 Humphrey cycle and the Joule cycle. These studies have shown that for TIT values above 1500°C, pressure gain above 1.6 would allow for at least 20% relative pressure drop in the plenum. The respective pressure gain becomes considerably higher for a TIT value of 1300°C. Based on these results, it is advisable to concentrate on TIT values above 1500°C to make the design of such a plenum easier. The results also show that the pressure drop requirement of the plenum depends only weakly on the cycle pressure ratio.

All results of the current work highlight a design path for future gas turbines with pressure-gain combustion. The new proposed cycle design not only enhances cycle efficiency but also applies a plenum between the combustion system and the turbine. This plenum will take over the task of conditioning the combustor exit flow and enable the operation of a conventional or slightly adapted turbine expander. The current work provides an initial estimation of the thermodynamic cost that can be allowed in this plenum to achieve efficiency gains with the Humphrey cycle.

ACKNOWLEDGMENT

The authors gratefully acknowledge the support by the Deutsche Forschungsge meinschaft(DFG) as part of the Collaborative Research Center SFB 1029 Substantial efficiency increase in gas turbines through direct use of coupled unsteady combustion and flow dynamics in project D01.

NOMENCLATURE

Latin characters

Bi	Biot number
C	Turbine cooling technology level constant
c_v	Specific heat capacity under constant volume kJ/kg K
c_p	Specific heat capacity under constant pressure kJ/kg K
K	Cooling air injection pressure loss constant
$\dot{m}$	Mass flow rate kg/s
T_A	Combustor inlet temperature K
T_{aw}	Blade wall temperature K
T_B	Combustor temperature at the end of the heat addition process K
T_{co}	Cooling air temperature K
T_3	Combustor outlet temperature K
T_{gi}	Temperature of the hot gas entering a turbine stage K
T_{int}	Intermediate temperature to compute the products' properties K
p_A	Combustor inlet pressure bar
p_B	Combustor pressure at the end of the heat addition process bar
p_3	Combustor outlet pressure bar
Q	Heat added through combustion W
δp_{mix}	Relative pressure drop due to cooling air mixing in the main exhaust stream % of p_{in}
δp_{plenum}	Plenum pressure loss coefficient
T_{bl}	Blade temperature used for cooling air calculations K
w	Specific work W
W^+	Temperature difference ratio -

Greek letters

γ	Specific heat capacity ratio
ϵ_f	Turbine stage film cooling effectiveness
ϵ_0	Overall turbine stage cooling effectiveness
η_{isC}	Compressor isentropic efficiency
η_{isPGC}	Combustor-internal isentropic efficiency
$\eta_{Cooling}$	Cooling air efficiency
η_{isT}	Turbine stage isentropic efficiency
η_{th}	Cycle thermal efficiency
Π_{C1}	Pressure ratio of compressor 1
$\Pi_{T-stage}$	Pressure ratio of turbine stage
ϕ	Combustion equivalence ratio
ξ	Cooling air ratio

ABBREVIATIONS

DME, Dimethyl ether; PGC, Pressure-gain combustion; PDC, Pulsed detonation combustion; PDE, Pulsed detonation engine; RDC, Rotating detonation combustion; SEC, Shockless explosion combustion; TIT, Turbine inlet temperature; ZND, Zeldovich, von Neumann, Dörring.

ORCID

Panagiotis Stathopoulos https://orcid.org/0000-0001-7008-3970

REFERENCES

1. Paxson D, Dougherty K. Ejector enhanced pulsejet based pressure gain combustors: an old idea with a new twist. In: *41st AIAA/ASME/SAE/ASEE Joint Propulsion Conference & Exhibit*; 2005.
2. Paxson DE. A simplified model for detonation based pressure-gain combustors. In: *46th AIAA/ASME/SAE/ASEE Joint Propulsion Conference & Exhibit, Nashville, Tennessee*; 2010:1-11.
3. Neumann N, Peitsch D. Potentials for pressure gain combustion in advanced gas turbine cycles. *Appl Sci*. 2019;9(16):3211.
4. Bach E, Stathopoulos P, Paschereit CO, Bohon MD. Performance analysis of a rotating detonation combustor based on stagnation pressure measurements. *Combust Flame*. 2020;217:21-36.
5. Kaemming TA, Paxson DE. Determining the pressure gain of pressure gain combustion. In: *Joint Propulsion Conference*; 2018.
6. Rankin BA, Fotia M, Paxson DE, Hoke J, Schauer F. Experimental and numerical evaluation of pressure gain combustion in a rotating detonation engine. In: *53rd AIAA Aerospace Sciences Meeting*; 2015.
7. Bratkovich T, Bussing T. A pulse detonation engine performance model. In: *31st Joint Propulsion Conference and Exhibit*; 1995.
8. Wintenberger E, Shepherd JE. A model for the performance of air-breathing pulse detonation engines. *J Propul Power*. 2006;22(3):593-603.
9. Ma F, Choi J-Y, Yang V. Propulsive performance of airbreathing pulse detonation engines. *J Propul Power*. 2006;22(6):1188-1203.
10. Heiser W, Pratt D. Thermodynamic cycle analysis of pulse detonation engines. *J Propul Power*. 2002;18(1):68-76.
11. Cambier JL, Tegner JK. Strategies for pulsed detonation engine performance optimization. *J Propul Power*. 1998;14(4):489-498.
12. Goldmeer J, Tangirala V, Dean A. System-level performance estimation of a pulse detonation based hybrid engine. *J Eng Gas Turb Power*. 2008;130(1):011201-011209.
13. Vutthivithayarak R. *Analysis of pulse detonation turbojet engines*. PhD thesis. University of Texas at Arlington; 2011.
14. Stathopoulos P. Comprehensive thermodynamic analysis of the Humphrey cycle for gas turbines with pressure gain combustion. *Energies*. 2018;11(12):3521
15. Nalim MR. Thermodynamic limits of work and pressure gain in combustion and evaporation processes. *J Propul Power*. 2002;18(6):1176-1182.
16. Paxson D, Kaemming T. Foundational performance analyses of pressure gain combustion thermodynamic benefits for gas turbines. In: *50th AIAA Aerospace Sciences Meeting Including the New Horizons Forum and Aerospace Exposition, Nashville, Tennessee*; 2012.
17. Paxson DE, Kaemming T. Influence of unsteadiness on the analysis of pressure gain combustion devices. *J Propul Power*. 2014;30(2):377-383.
18. Rähse T, Paschereit C, Stathopoulos P, Berndt P, Klein R. Gas dynamic simulation of shockless explosion combustion for gas turbine power cycles. In: *Proceedings of the ASME Turbo Expo*, Vol. 3; 2017.
19. Rähse TS, Stathopoulos P, Schäpel J-S, Arnold F, King R. On the influence of fuel stratification and its control on the efficiency of the shockless explosion combustion cycle. In: *Proceedings of ASME Turbo Expo, ASME International, Oslo, Norway*; 2018.
20. Gray J, Vinkeloe J, Moeck J, et al. Thermodynamic evaluation of pulse detonation combustion for gas turbine power cycles. In: *Proc. Turbo Expo. 2016, ASME*; 2016.
21. Nordeen CA, Schwer D, Schauer F, Hoke J, Barber T, Cetegen B. Thermodynamic model of a rotating detonation engine. *Combust Explos Shock Waves*. 2014;50(5):568-577.
22. Zhou R, Wang J-P. Numerical investigation of flow particle paths and thermodynamic performance of continuously rotating detonation engines. *Combust Flame*. 2012;159(12):3632-3645.
23. Kaemming T, Fotia ML, Hoke J, Schauer F. Thermodynamic modeling of a rotating detonation engine through a reduced-order approach. *J Propul Power*. 2017;33(5):1-9.
24. Mizener AR, Lu FK. Preliminary parametric analysis of a rotating detonation engine by analytical methods. In: *52nd AIAA/SAE/ASEE Joint Propulsion Conference, American Institute of Aeronautics and Astronautics, Reston, Virginia*; 2016.
25. Sousa J, Paniagua G, Collado Morata E. Thermodynamic analysis of a gas turbine engine with a rotating detonation combustor. *Appl Energy*. 2017;195:247-256.
26. Naples JL, Fotia AG, Theuerkauf ML, Hoke S, Schauer FR. Design and testing of a rotating detonation engine for open-loop gas turbine integration. In: *25th ICDERS*; 2015:2-7.
27. Naples A, Hoke J, Battelle RT, Wagner M, Schauer FR. RDE implementation into an open-loop T63 gas turbine engine. In: *55th AIAA Aerospace Sciences Meeting, American Institute of Aeronautics and Astronautics, Reston, Virginia*; 2017.
28. Naples A, Battelle R, Hoke J, Schauer F. T63 turbine response to rotating detonation combustor exhaust flow. In: *Proceedings of ASME Turbo Expo, ASME*; 2018.
29. Braun EM, Lu FK, Wilson DR, Camberos JA. Airbreathing rotating detonation wave engine cycle analysis. *Aerosp Sci Technol*. 2013;27(1):201-208.
30. Ji Z, Zhang H, Wang B. Performance analysis of dual-duct rotating detonation aero-turbine engine. *Aerosp Sci Technol*. 2019;92:806-819.
31. Stathopoulos P, Rähse T, Vinkeloe J, Djordjevic N. First law thermodynamic analysis of the recuperated Humphrey cycle for gas turbines with pressure gain combustion. *Energy*. 2020;200:117492.
32. Mizener AR, Lu FK, Rodi PE. Performance sensitivities of rotating detonation engines installed onto waverider forebodies. *J Propul Power*. 2019;35(2):289-302.
33. Rasheed A, Furman AH, Dean AJ. Experimental investigations of the performance of a multitube pulse detonation turbine system. *J Propul Power*. 2011;27(3):586-596.
34. Glaser A, Caldwell N, Gutmark E. Performance of an axial flow turbine driven by multiple pulse detonation combustors. In: *45th AIAA Aerospace Sciences Meeting and Exhibit*, 2012.
35. Fernelius MH, Gorrell SE. Mapping efficiency of a pulsing flow-driven turbine. *J Fluids Eng*. 2020;142(6):61202.
36. Xisto C, Petit O, Grönstedt T, Rolt A, Lundbladh A, Paniagua G. The efficiency of a pulsed detonation combustor-axial turbine integration. *Aerosp Sci Technol*. 2018;82:80-91.
37. Reichel TG, Schäpel J-S, Bobusch BC, Klein R, King R, Oliver Paschereit C. Shockless explosion combustion: experimental investigation of a new approximate constant volume combustion process. *J Eng Gas Turb Power*. 2016;139(2):21504.
38. Yücel F, Völzke F, Paschereit C. Effect of the switching times on the operating behavior of a shockless explosion combustor. In: King R, editor. *Active Flow and Combustion Control, Notes on Numerical Fluid Mechanics and Multidisciplinary Design*. Cham, Switzerland: Springer Nature Switzerland AG;2018:121-134.
39. Berndt P. *Mathematical modeling of the shockless explosion combustion*. Ph.D. thesis. Freie Universität Berlin; 2016.

40. Burke MP, Chaos M, Ju Y, Dryer FL, Klippenstein SJ. Comprehensive H2/O2 kinetic model for high-pressure combustion. *Int J Chem Kinet*. 2011;44(7):444-474.
41. Kurzke J. *GasTurb 12 Design and Off-Design Performance of Gas Turbines*. GasTurb GmbH; 2015.
42. Horlock J, Watson D, Jones T. Limitations on gas turbine performance imposed by large turbine cooling flows. *J Eng Gas Turbines Power*. 2001;123(3):487-494.
43. Horlock JH, Torbidoni L. Calculations of cooled turbine efficiency. *J Eng Gas Turb Power*. 2008;130(1):011703 -011708.
44. Wilcock R, Young J, Horlock J. The effect of turbine blade cooling on the cycle efficiency of gas turbine power cycles. *J Eng Gas Turbines Power*. 2005;127(1):109-120.
45. Matzen M, Demirel Y. Methanol and dimethyl ether from renewable hydrogen and carbon dioxide: alternative fuels production and life-cycle assessment. *J Clean Prod*. 2016;139:1068-1077.
46. Gentzen M, Doronkin D, Sheppard T, Grunwaldt J-D, Sauer J, Behrens S. An intermetallic Pd2Ga nanoparticle catalyst for the single-step conversion of CO-rich synthesis gas to dimethyl ether. *Appl Catal A*. 2018;562:206-214.

How to cite this article: Stathopoulos P. An alternative architecture of the Humphrey cycle and the effect of fuel type on its efficiency. *Energy Sci Eng*. 2020;00:1–15. https://doi.org/10.1002/ese3.776

APPENDIX A

From the internal Nu number to the required blade cooling mass flow

The Nusselt number inside the turbine blades is not directly used for models of the secondary air system in gas turbines. The approach of Horlock[42] and Wilcock[44] that considers convective cooling and film cooling is used in the current work.

The internal cooling efficiency $\eta_{Cooling}$ can be determined from the internal heat transfer.[42] If a constant blade temperature T_{bl} is assumed, the cooling efficiency can be defined as follows:

$$\eta_{Cooling} = \frac{T_{co} - T_{ci}}{T_{bl} - T_{ci}} = 1 - \exp\left(-St_c \frac{A_{sc}}{A_c}\right) \tag{7}$$

where St_c is the internal Stanton number and A_{sc} and A_c are the surface and cross-sectional areas of the coolant channel in the blade. If in addition the Reynolds Re and Prandtl Pr numbers are assumed constant in the various cycle configurations, the Stanton number St_c, defined in Equation (8), is only a function of the Nu number. As a result, also the internal cooling efficiency $\eta_{Cooling}$ can be expressed as a function of Nusselt number only.

$$St_c = \frac{Nu}{Re \cdot Pr} \tag{8}$$

This internal cooling efficiency is used to compute the temperature difference ratio (W^+) for convective and film cooling.

1. Convective cooling:

$$W^+ = \frac{\varepsilon_0}{\eta_{Cooling}\left(1 - \varepsilon_0\right)} \tag{9}$$

2. Convective and film cooling:

$$W^+ = \frac{\varepsilon_0 - \left(1 - \eta_{Cooling}\right)\varepsilon_f - \varepsilon_0 \varepsilon_f \eta_{Cooling}}{\eta_{Cooling}\left(1 - \varepsilon_0\right)} \tag{10}$$

The film cooling effectiveness in Equation (10) is defined as follows:

$$\varepsilon_f = \left(T_{gi} - T_{aw}\right) / \left(T_{gi} - T_{co}\right) \tag{11}$$

The film cooling effectiveness is generally set equal to 0.4 based on experimental data,[42] while the overall cooling effectiveness ε_0 in Equations (9) and (10) is defined as follows:

$$\varepsilon_0 = \left(T_{gi} - T_{bl}\right) / \left(T_{gi} - T_{ci}\right) \tag{12}$$

where T_{bl} is the blade temperature. The variable B in Equation (10) is defined as follows:

$$B = 1 - \frac{\varepsilon_0 - \varepsilon_f}{1 - \varepsilon_0} \cdot Bi_{Met} \tag{13}$$

The Biot numbers are typically considered constant[44] and the required cooling air ratio ξ for the blade row in question if finally computed from

$$\xi = \frac{\dot{m}_c}{\dot{m}_{gi}} = C \cdot W^+ \tag{14}$$

In this equations, C is a constant indicative of the "level of technology" and it is a free parameter used to adapt this model to different technological advancements of the cooling methods, without changing its basic architecture.